Exponential and nonexponential buildup in resonant tunneling

Roberto Romo,[1,*] Alberto Hernández,[2] and Jorge Villavicencio[1]

[1]*Facultad de Ciencias, Universidad Autónoma de Baja California, Apartado Postal 1880, 22800 Ensenada, Baja California, México*

[2]*Centro de Ingeniería y Tecnología, Universidad Autónoma de Baja California, Unidad Valle de las Palmas, Tijuana, Baja California, México*

(Received 10 January 2013; published 27 February 2013)

The exponential and nonexponential regimes of the buildup process in resonant tunneling structures are analyzed by considering an analytic solution of the time-dependent Schrödinger equation. It is found that the buildup exhibits a purely exponential behavior in a finite time interval followed by a clear transition to a nonexponential regime. The buildup of the probability amplitude in the nonexponential regime follows a $t^{-3/2}$ time dependence, in the same fashion as the survival amplitude in quantum decay. For incidence energies at higher isolated resonances, $E = \varepsilon_n$ with $n > 1$, it is found that the exponential regime is split into two exponential subregimes: the first one is governed by the width Γ_n of the resonance chosen for the incidence energy, and the second one is dominated by the width Γ_1 of the lowest resonance. The transition occurs directly from n to 1 without jumps to other intermediate resonant states. This dynamics is discussed in comparison with the (opposite) and well-studied process of quantum decay, with which we find that there are striking similarities in both the exponential and nonexponential regimes. We also analyze the buildup in systems with resonance doublets, where the interference effects produced by the interacting resonances play an important role. In the latter case we find that the buildup of the probability amplitude exhibits a complex oscillatory behavior that can be characterized by a mix of oscillating contributions with well-defined Rabi type frequencies of the form $|E - \varepsilon_n|/\hbar$, where ε_n are the nearest resonances around the incidence energy E.

DOI: 10.1103/PhysRevA.87.022121 PACS number(s): 03.65.Xp, 73.21.Cd, 73.40.Gk

I. INTRODUCTION

The study of transient phenomena in quantum tunneling has received a great deal of attention in recent years [1], motivated in part by the advent of technological advances in the design of artificial quantum structures [2,3], which opened new ways to study the time evolution of scattering and decay in quantum systems. On the other hand, the transients have frequently been studied *per se* due to their interesting dynamics, and because they are often used to clarify fundamental questions of time-dependent quantum processes. In the context of resonant tunneling (RT), the understanding of transients has become essential because they allow for the exploration of the dynamics of tunneling phenomena at their earliest stages, where there have been a number of recent works studying transport processes and related issues [4–10].

The *buildup* of electronic states in quantum wells is one of the most important transient processes in RT because it governs the dynamics of electron transport. One of the first studies of the filling up of the electronic probability density in one-dimensional systems was performed by Kleber [11] in a double-δ potential and provided analytical solutions for both the internal and external regions of the system. There are also studies of the buildup dynamics in double-barrier systems [10, 12–16] and multibarrier resonant structures using Gaussian wave packets [17–19] that explore its transients. However, the dynamics of the buildup has not been explored in such depth as its counterpart, *quantum decay*. Unlike the buildup, which deals with the flux of particles coming into the quantum structure, quantum decay is related to particle escape out of an interaction region with a confining potential, so in this sense they are opposite processes. The study of the latter originated in the early days of quantum mechanics [20,21], establishing the well-known exponential decay law. Subsequent work by Khalfin [22] at the end of the 1950s led to the prediction of nonexponential decay, confirmed experimentally in recent years for both the short- and the long-time regimes [23,24]. Even though buildup and decay are quite different physical processes, their dynamics exhibits striking similarities that have not been fully explored. In Ref. [13] the existence of exponential and nonexponential contributions in the buildup process, in the same fashion as in quantum decay, is briefly mentioned, but there has not been further study on this issue.

In this paper we study the dynamics of the buildup process of the probability density in resonant tunneling structures for cut-off incident plane waves. Two different situations are considered in the present study: (i) the simple case of incidence at an isolated resonance, with special emphasis on the case of incidence at higher resonances ($E = \varepsilon_n$, $n > 1$); (ii) incidence in the vicinity of a resonance doublet, which is typical of systems of two quantum wells coupled through a central barrier. Our study of the buildup has the characteristic of being conducted in comparison with the quantum decay phenomenon, pointing out the similarities as well as the fundamental differences.

The paper is organized as follows. In Sec. II we present the formal solution of the problem, and also the derivation of an analytical expression for the probability density valid for the exponential region. Section III deals with numerical examples of the buildup dynamics in systems with isolated resonances as well as in systems with resonance doublets. Finally, in Sec. IV we present the concluding remarks.

II. FORMALISM

For this kind of analysis it is necessary to have an adequate formalism that can provide detailed information about the

*romo@uabc.edu.mx

contributions of each of the resonant states and their mutual interference to the time-dependent probability density. In the present study we use a resonance formalism capable of providing us with this detailed information. In this section we present a brief résumé of the resonant-state formalism employed to describe the time evolution of the wave function in the internal region of the system.

A. The formal solution

Our analysis is based on the solution of the time-dependent Schrödinger equation

$$\left(i\hbar\frac{\partial}{\partial t}-H\right)\Psi=0 \tag{1}$$

for potentials of arbitrary shape that vanish outside the region $0\leqslant x\leqslant L$, under the quantum-shutter initial condition, represented by [25]

$$\Psi(x,k;t=0)=\begin{cases}e^{ikx}-e^{-ikx}, & -\infty<x\leqslant 0,\\ 0, & x>0.\end{cases} \tag{2}$$

Once the shutter is suddenly removed at $t=0$, the initial wave is enabled to interact with the potential, allowing us to analyze step by step the spatial and time evolution of the buildup of the electronic probability density in the quantum wells of the system. For this setup, the solution throughout the internal region is given by [25]

$$\Psi(x,k;t)=\phi(x,k)M[y(k,t)]-\phi^{*}(x,k)M[y(-k,t)]-\sum_{n=-\infty}^{\infty}\rho_n(x,k)M[y(k_n,t)], \tag{3}$$

where $k_n\equiv a_n-ib_n$ $(a_n,b_n>0)$ are the poles of the outgoing Green's propagator of the problem in both the fourth $(n>0)$ and third $(n<0)$ quadrants of the complex k plane. The function $\phi(x,k)$ is the solution of the time-independent Schrödinger equation and hence represents the stationary situation at asymptotically long times. The coefficients of the sum, $\rho_n(x,k)$, are given in terms of the resonance eigenfunctions $u_n(x)$ and eigenvalues k_n, by

$$\rho_n(x,k)=2ik\frac{u_n(0)u_n(x)}{k^2-k_n^2}. \tag{4}$$

To compute these coefficients we basically need to calculate the complex poles k_n of the outgoing Green's propagator and the resonant states $u_n(x)$, which are solutions of the time-independent Schrödinger equation with outgoing boundary conditions [26].

The time dependence of the solution given by Eq. (3) is contained in the Moshinsky functions $M(y)$, defined as

$$M(y_q)=\tfrac{1}{2}w(iy_q), \tag{5}$$

where $w(z)=\exp(-z^2)\mathrm{erfc}(-iz)$ is the complex error function [27]. The argument y_q depends on the time through the relation

$$y(q,t)=-e^{-i\pi/4}\left(\frac{m}{2\hbar t}\right)^{1/2}\left[\frac{\hbar q}{m}t\right], \tag{6}$$

where q stands for $\pm k$ or $k_{\pm n}$.

The formal solution, Eq. (3), involves the contribution of the full resonant spectrum of the system, and can be used to calculate the probability density $|\Psi(E,x;t)|^2$ for $0\leqslant x\leqslant L$, at any time t and incidence energy E, provided that the relevant sets of resonant states $\{u_n\}$ and complex eigenvalues $\{k_n\}$ of the system are known. This evaluation involves in principle an infinite set of resonance terms, but in practice we use a finite number N of resonance eigenfunctions $u_n(x)$ and poles k_n and obtain an approximation $\Psi_N(x,k;t)$ to Eq. (3), namely,

$$\Psi\approx\Psi_N\equiv\phi M[y(k,t)]-\phi^{*}M[y(-k,t)]-\sum_{n=1}^{N}\{\rho_n M[y(k_n,t)]+\rho_{-n}M[y(k_{-n},t)]\}. \tag{7}$$

To evaluate the contributions of the third quadrant, we can use the symmetry properties $k_{-n}=-k_n^{*}$ and the time-reversal invariance of the eigenfunctions u_n i.e., $u_{-n}(x)=u_n^{*}(x)$ [10].

B. Exponential contributions

In this section we use some analytical properties of the Moshinsky functions to derive a simple analytical formula that describes the different exponential contributions to the probability density associated with the resonant states and their interferences. Using in Eq. (7) the N-term approximation to the stationary wave function [26]

$$\phi(x,k)\approx\phi_N(x,k)\equiv\sum_{n=1}^{N}\rho_n(x,k), \tag{8}$$

and the symmetry relation [10]

$$M(y)=e^{y^2}-M(-y) \tag{9}$$

of the Moshinsky functions $M[y(k,t)]$ and $M[y(k_n,t)]$, and noting that $-y(q,t)=y(-q,t)$, we can obtain an expression for Ψ_N where all the Moshinsky functions have complex arguments $y=|y|\exp i\theta$ that have a phase lying in the interval $-\pi/2<\theta<\pi/2$. This kind of Moshinsky function can be represented by a series expansion of the form $M(y)\sim(1/2)[1/(\pi^{1/2}y)-1/(\pi^{1/2}y^3)+\cdots]$, which is a decreasing function of time. Therefore, an alternative expression for Ψ_N is

$$\Psi_N=\sum_{n=1}^{N}\rho_n(x,k)\left[e^{[y(k,t)]^2}-e^{[y(k_n,t)]^2}\right]+B(x,k;t), \tag{10}$$

where $B(x,k;t)$ is a background term that contains the nonexponential contribution through the M functions, which can be represented by the above series expansion and hence are also decreasing functions of time as inverse powers of t [10].

After simple algebra, an analytic expression for the probability density can be calculated from Eq. (10), which becomes

$$P(E,x,t)\approx\sum_{n=1}^{N}\mathcal{P}_n(E,x,t)+\sum_{n<m}^{N}\mathcal{P}_{mn}(E,x,t), \tag{11}$$

where we have ignored all the nonexponential contributions coming from $B(x,k;t)$. Here, $\mathcal{P}_n(E,x,t)$ and the interference terms $\mathcal{P}_{mn}(E,x,t)$ are given, respectively, by

$$\mathcal{P}_n(E,x,t)=|\rho_n|^2\chi_n(E,t) \tag{12}$$

and

$$\mathcal{P}_{mn}(E,x,t) = 2\mathrm{Re}[\rho_n \rho_m^* \xi_{mn}(E,t)], \tag{13}$$

where the time dependence is contained in the functions

$$\chi_n(t) = 1 - 2e^{-\Gamma_n t/2\hbar}\cos\hat{\omega}_n t + e^{-\Gamma_n t/\hbar}, \tag{14}$$

$$\xi_{mn}(t) = 1 - e^{-i\hat{\omega}_n t}e^{-\Gamma_n t/2\hbar} - e^{i\hat{\omega}_m t}e^{-\Gamma_m t/2\hbar} + e^{i\hat{\omega}_{mn} t}e^{-(1/2)(\Gamma_m+\Gamma_n)t/\hbar}. \tag{15}$$

We have defined $\hat{\omega}_n = (E-\varepsilon_n)/\hbar$ and $\hat{\omega}_{mn} = (\varepsilon_m - \varepsilon_n)/\hbar$; their absolute values are Rabi-type frequencies. Here, ε_n and Γ_n are the energy and width of the nth resonance $E_n \equiv \varepsilon_n - i\Gamma_n/2 = \hbar^2 k_n^2/2m$.

Notice that the probability density given in Eq. (11), in the limit of asymptotically long times, gives (for $x = L$) the transmission coefficient. That is, $P(E,L,t\to\infty) \to T(E)$, where

$$T(E) = \sum_{n=1}^{N} T_n(E) + \sum_{n<m}^{N} T_{mn}(E), \tag{16}$$

which coincides with Eq. (5) of Ref. [26]; $T_n(E)$ and $T_{mn}(E)$ have exactly the expressions given by Eqs. (6) and (10) of that reference.

III. EXPONENTIAL AND NONEXPONENTIAL BUILDUP

The buildup dynamics at a given incidence energy E crucially depends on how the system's resonances near E are distributed. Quite different behaviors are expected, for example, for incidence at an isolated resonance and at a resonance doublet, or at something more complex such as a miniband where various resonances are packed together. In the following two sections we treat separately the case of incidence at a single isolated resonance and the case where the resonances are grouped in pairs. We shall analyze the behavior of the quantity $\Delta = |1 - |\Psi/\phi||$ as a function of time t, which measures how close is $|\Psi(x,t)|$ to reaching its asymptotic limit $|\phi(x)|$ at a given position and time. It turns out to be convenient to plot the logarithm of Δ to distinguish more clearly the exponential from the nonexponential behavior in the dynamics of the buildup process.

A. Incidence at an isolated resonance

We analyze here the exponential and nonexponential contributions to the buildup for the special case of incidence at a given resonance energy of the system, $E = \varepsilon_n$. Let us first consider the case of incidence at the lowest resonance, $n = 1$. The cases with $n > 1$ exhibit different behavior and are treated separately below.

Let us consider the double-δ system with barrier intensities $\lambda = 5.0$ eV nm and barrier separation $b = 8.0$ nm. The resonance energies and widths of the first few resonances are $\varepsilon_1 = 83.02$ meV, $\Gamma_1 = 0.398$ meV, $\varepsilon_2 = 332.22$ meV, $\Gamma_2 = 3.154$ meV, $\varepsilon_3 = 747.98$ meV, $\Gamma_3 = 10.47$ meV, $\varepsilon_4 = 1.33$ eV, $\Gamma_4 = 24.28$ meV, $\varepsilon_5 = 2.08$ eV, and $\Gamma_5 = 46.15$ meV. For incidence energy at the lowest resonance $E = \varepsilon_1$, we show in Fig. 1(a) the evolution of $|\Psi/\phi|^2$ as a function of time at a fixed position $x = L/2$. As we can see, the probability density exhibits a smooth gradual increase towards its asymptotic value $|\phi|^2$. The inset shows snapshots of the buildup of the probability density inside the system at different times (blue dashed lines) and compared with the stationary probability density $|\phi|^2$ (red solid line). As we can see, the buildup is characterized by a monotonic increase.

In order to exhibit the exponential and nonexponential contributions, we present in Fig. 1(b) a plot of $\ln\Delta$ vs t at $x = L/2 = 4.0$ nm, using Eq. (7) with $N = 1000$ resonance terms of the series. We clearly appreciate in this graph that there exists a time regime where $\ln\Delta$ exhibits a linear time dependence that perfectly coincides with the straight line with slope $m_1 = -\Gamma_1/2\hbar$ (red dashed line). The above means that the buildup is purely exponential in this time interval and governed by Γ_1. At long enough times, the buildup departs from this purely exponential behavior occurring a transition from exponential to a (nonexponential) power law (at approximately 80 ps). As is well known, in quantum decay the nonexponential regime of the survival amplitude $A(t)$ at long times is characterized by the time dependence $|A(t)| \sim t^{-3/2}$ [28]. In order to investigate whether the buildup process follows a similar time dependence in the non-exponential region, we use the auxiliary function

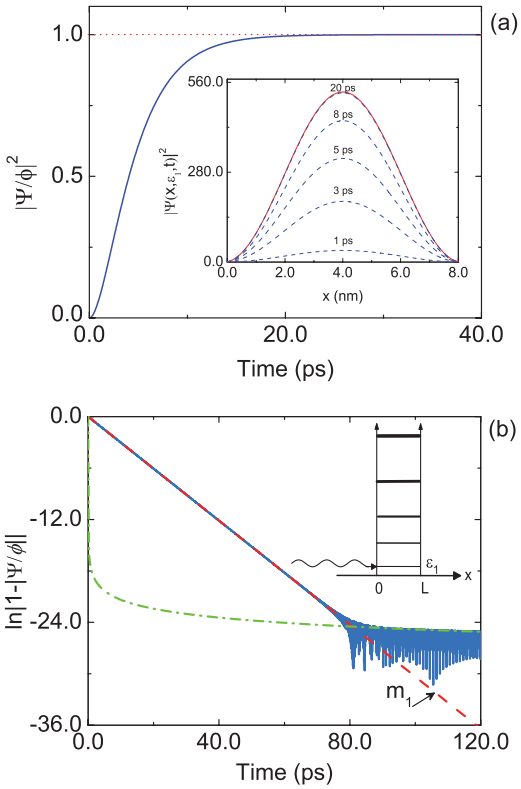

FIG. 1. (Color online) (a) Time evolution of $|\Psi/\phi|^2$ at $x = L/2 = 4.0$ nm for incidence energy at the first resonance, $E = \varepsilon_1 = 83.02$ meV, in a symmetrical double-δ potential. The inset shows snapshots of $|\Psi|^2$ vs x at different fixed times (blue dashed lines), where the stationary probability density $|\phi|^2$ is included for comparison (red solid line). (b) Plot of $\ln|1 - |\Psi/\phi||$ vs t at $x = L/2$. The exponential regime is dominated by the first resonance as is evident from the red dashed straight line (included to help the eye) which has slope $m_1 = -\Gamma_1/2\hbar$. The green dash-dotted curve (also included to help the eye) is the logarithm of a function $f(t)$ that varies as $t^{-3/2}$.

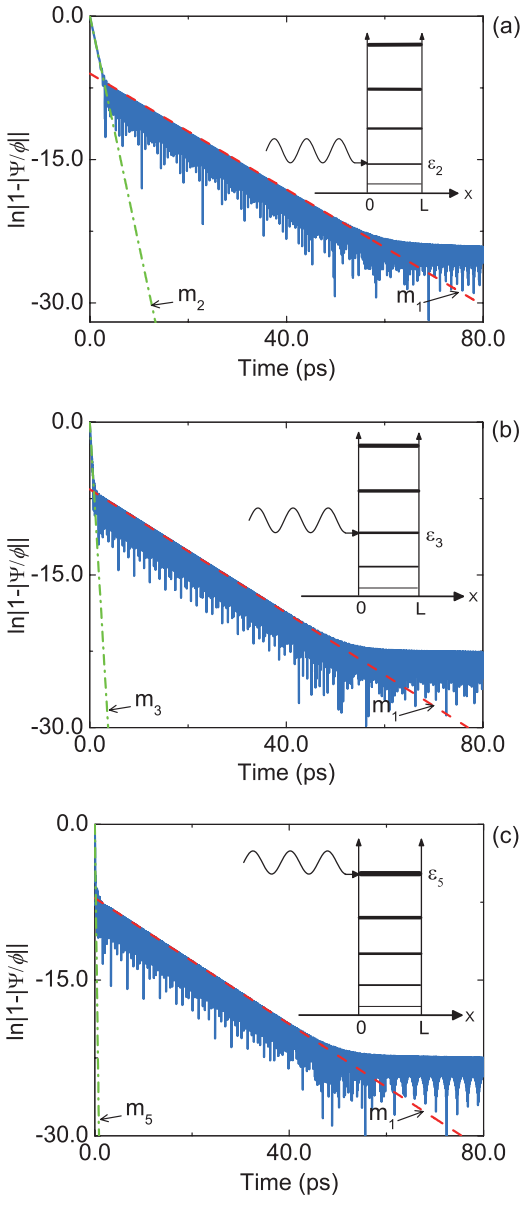

FIG. 2. (Color online) Exponential and nonexponential contributions to the buildup process for incidence at different resonance energies: (a) $E = \varepsilon_2$, (b) $E = \varepsilon_3$, and (c) $E = \varepsilon_5$. In all cases the exponential regime is split into two exponential subregimes, the first dominated by the resonance at incidence and the second by the first resonance. The red dashed straight lines have slopes $-\Gamma_n/2\hbar$ and $-\Gamma_1/2\hbar$, respectively, and are included to help the eye.

$f(t) = (1+\alpha t)^{-3/2}$ where $\alpha = 1.53 \times 10^5$ ps^{-1} is a fitting parameter. The comparison of the ln Δ vs t graph (blue solid line) with the graph of ln $f(t)$ vs t (green dash-dotted line) shows that the nonexponential regime of the buildup also varies as $t^{-3/2}$. Other striking similarities with the decay process also occur in the exponential regime and are discussed below.

Let us consider now incidence at higher resonances ($n > 1$). In Fig. 2 we present the results for the cases (a) $E = \varepsilon_2$, (b) $E = \varepsilon_3$, and (c) $E = \varepsilon_5$. In contrast to the case $E = \varepsilon_1$ of the previous figure, we clearly see that the exponential regime here is split into two subregimes: the first one coincides with the straight line with slope $m_n = -\Gamma_n/2\hbar$ (green dash-dotted lines) where n is the selected resonance for the incidence energy, and the second one coincides with the straight line with slope $m_1 = -\Gamma_1/2\hbar$ (red dashed line), associated with the lowest resonance. As we can see, these straight lines perfectly fit as envelopes of the ln Δ vs t graph in the two exponential subregimes. The above means that the buildup in the quantum well starts at the relatively high rate established by Γ_n, and then is suddenly slowed down at a transition point where the exponential buildup continues at the slower (still exponential) rate dictated by the first resonance width Γ_1, up to a second transition where it is slowed down again and enters into the nonexponential regime.

The most striking aspect of the observed behavior is the fact that the change occurs directly from the nth state to the ground state without jumping to intermediate states m ($1 < m < n$). Interestingly, a quite similar behavior occurs in quantum decay. There, when the initial state is placed at a higher resonance level ($n > 1$), it results in an exponential regime split into two exponential subregimes with a clear transition between them, followed by the well-known transition to nonexponential decay at long times. It was shown in Ref. [29] that the survival amplitude in the first exponential interval is governed by the resonance width Γ_n of the chosen initial state, while the second becomes governed by the resonance width Γ_1 of the ground state without intermediate transitions, and finally the decay is slowed down again, continuing at a nonexponential rate characterized by a $t^{-3/2}$ dependence. This is an interesting parallel between the two physical processes, considered as opposites in the sense that one deals with the incoming of electrons to the quantum wells and the other with their escape out of the system. The genesis of the common features between the buildup and the decay dynamics lies in the fact that the time evolution of both processes is described by the same kind of function, the Moshinsky functions. In our case, the exponential part was explicitly separated from the nonexponential contribution using the symmetry relation (9) in the functions $M[y(k_n,t)]$ and $M[y(k,t)]$. As a result, two exponential terms appear in Eq. (10), namely, $e^{[y(k,t)]^2}$ and $e^{[y(k_n,t)]^2}$. The former of these two terms is related to the incident wave, and hence is not present in the decay case. This is a fundamental difference, which leads to Rabi-type frequencies that involve the incidence energy E in the buildup process, as we shall show in the next section. We discuss below the origin of this behavior in the buildup case.

The existence of the two exponential subregimes exhibited in Fig. 2 can be explained using the analytic formulas given in Sec. II B. For the double-δ system, we have the hierarchy $\Gamma_1 < \Gamma_2 < \cdots < \Gamma_n$, which implies $e^{-\Gamma_1 t/2\hbar} > e^{-\Gamma_n t/2\hbar}$ at any time $t > 0$. However, each of these exponentials has in Eq. (12) a prefactor $|\rho_n|^2$ whose value depends on the difference $E - \varepsilon_n$, according to the expression

$$|\rho_n(x,E)|^2 = \frac{2\hbar^2 E}{m} \frac{|u_n(0)|^2 |u_n(x)|^2}{(E-\varepsilon_n)^2 + \Gamma_n^2/4}. \tag{17}$$

It is clear that the factor $|\rho_n(x,E)|^2$ has a maximum value when $E = \varepsilon_n$, and hence for incidence at the nth resonance we have $|\rho_n^2| \gg |\rho_1^2|$. As a consequence of the above, at the beginning of the exponential regime we have $\mathcal{P}_1(E,x,t) < \mathcal{P}_n(E,x,t)$, explaining the existence of the first exponential subregime

(dominated by Γ_n). As time goes on, the dominance of the exponential $e^{-\Gamma_1 t/2\hbar}$ over $e^{-\Gamma_n t/2\hbar}$ becomes so strong that the roles are inverted so that after a certain time we have $\mathcal{P}_1(E,x,t) > \mathcal{P}_n(E,x,t)$, giving rise to the second exponential subregime (governed by Γ_1). Only two states are capable of giving the leading contribution to the probability density, the state of incidence (for which $|\rho_n|^2$ attains a maximum value) and the ground state (which has the leading exponential). For example, in the case of $E = \varepsilon_5$ of Fig. 2(c), we have $|\rho_5/\rho_4|^2 = 2.1 \times 10^{34}$, $|\rho_5/\rho_3|^2 = 737.0$, $|\rho_5/\rho_2|^2 = 5.4 \times 10^{31}$, and $|\rho_5/\rho_1|^2 = 11.5$, which explains why only the states $n = 5$ and $n = 1$ are important here, and why the transition occurs directly from $n = 5$ to $n = 1$ without intermediate jumps. The extremely small values of ρ_2 and ρ_4 are due to the fact that the eigenstates $u_2(x)$ and $u_4(x)$ have a node at $L/2$. There are, however, situations where two (or more) resonances are so close that the corresponding coefficients have comparable values, and consequently two or more resonances share the leading contribution in the first exponential subregime. We discuss one example of these cases in the next section.

1. *Incidence at a resonance doublet*

We are now interested in analyzing the situation where more than one resonance take part in the process. This occurs when two or more resonances are so close to each other that the interference contributions in the probability density cannot be ignored. An appropriate example to explore this case is a system with two quantum wells coupled by a central barrier. We use here a symmetrical triple-δ potential with barrier intensities $\lambda = 5.0$ eV nm, and barrier separations $b = 8.0$ nm, whose corresponding distribution of resonances in the complex energy plane is illustrated in Fig. 3 (solid dots). Instead of isolated resonances, we see that the spectrum is characterized by pairs of neighboring resonances of similar positions and widths.

In order to analyze the exponential and nonexponential contributions, Fig. 4(a) illustrates the behavior of $\ln \Delta$ vs t

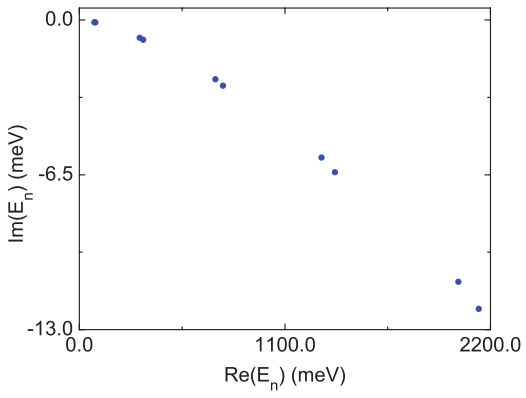

FIG. 3. (Color online) First ten poles $E_n = \varepsilon_n - i\Gamma_n/2$ of the outgoing Green's function propagator on the complex energy plane for a symmetrical triple-δ potential with barrier intensities $\lambda = 5.0$ eV nm and barrier separations $b = 8.0$ nm. The resonance energies and widths of the first few resonances are $\varepsilon_1 = 80.77$ meV, $\Gamma_1 = 0.188$ meV, $\varepsilon_2 = 85.36$ meV, $\Gamma_2 = 0.211$ meV, $\varepsilon_3 = 323.30$ meV, $\Gamma_3 = 1.49$ meV, $\varepsilon_4 = 341.53$ meV, and $\Gamma_4 = 1.66$ meV.

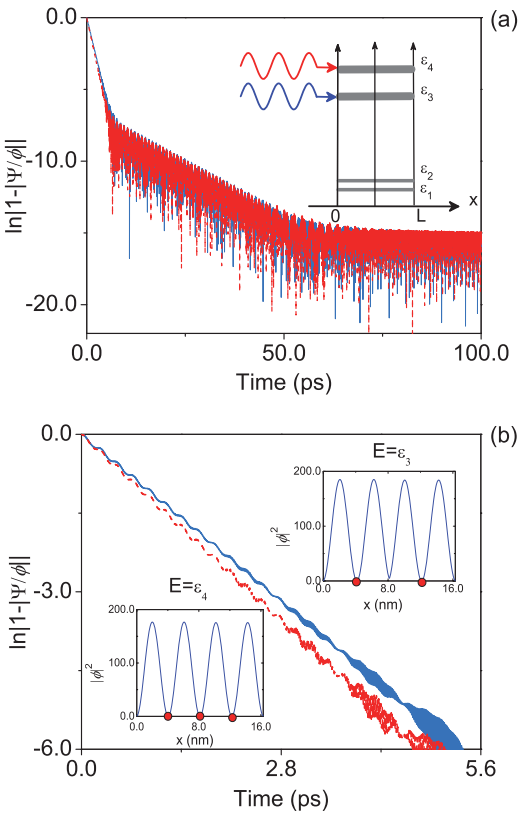

FIG. 4. (Color online) (a) Exponential and nonexponential contributions to the buildup process for incidence at $E = \varepsilon_3$ (solid blue line) and $E = \varepsilon_4$ (dashed red line) of a triple-barrier resonant structure, as pictured in the inset. (b) The same as in (a) in a shorter interval in the first exponential region. The linear behaviors have similar slopes $m_3 \approx m_4$ since $\Gamma_3 \approx \Gamma_4$. The insets show the stationary (asymptotic) probability density for each of the incidence energies; they look almost identical but one of them has three nodes and the other only two (red solid circles).

at the fixed position $x_f = 10.0$ nm for incidence at $E = \varepsilon_3$ (solid blue line) and $E = \varepsilon_4$ (dashed red line) as pictured in the inset. The behavior is essentially the same for both incidence energies, for the corresponding graphs are almost indistinguishable as seen in Fig. 4(a). Only if we make an amplification of the graphs in a shorter interval can the curves be distinguished one from the other, as we can see in the expanded view shown in Fig. 4(b), where linear behaviors with tiny oscillations for both incidence energies can be clearly appreciated. In contrast to the double-δ case of the previous section where the resonances widths are quite different, here we have $\Gamma_3 \approx \Gamma_4$ and hence the corresponding slopes $m_n = -\Gamma_n/2\hbar$ of the curves almost coincide, $m_3 \approx m_4$. These exponential behaviors, governed by Γ_3 and Γ_4, end at approximately $t = 7$ ps, where another exponential regime (governed by Γ_1) begins, which, as shown in Fig. 4(a), is characterized by an oscillating curve modulated by a straight line with a (less pronounced) slope m_1. These lines are extended to approximately $t = 60$ ps, where a transition to a nonexponential regime occurs.

The explanation of these transitions is similar to the one given in the previous section for the case of isolated resonances, but with an important difference: instead of a

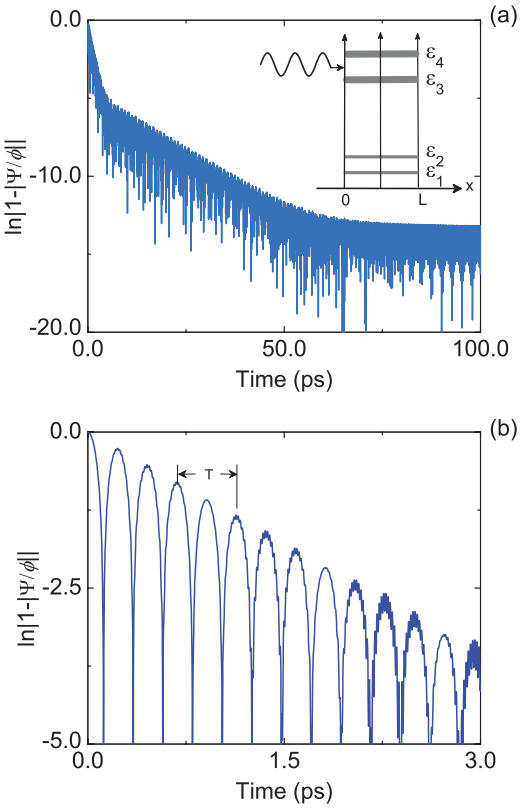

FIG. 5. (Color online) (a) Exponential and nonexponential contributions to the buildup process for off-resonance incidence at $E = (1/2)(\varepsilon_3 + \varepsilon_4) = 332.42$ meV of a triple-barrier resonant structure. (b) The same as in (a) in a shorter interval.

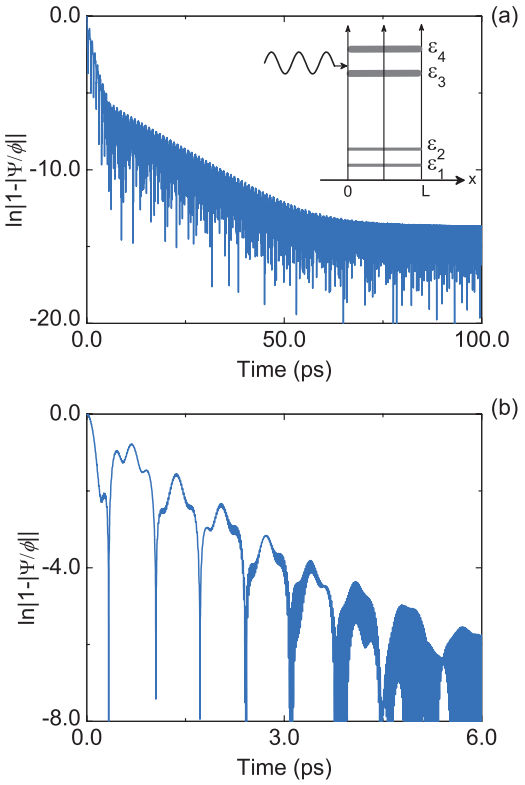

FIG. 6. (Color online) (a) Exponential and nonexponential contributions to the buildup process for off-resonance incidence at $E = \varepsilon_3 + 2\Gamma_3 = 326.28$ meV of a triple-barrier resonant structure. (b) The same as in (a) in a shorter interval.

single coefficient ρ_n there are two coefficients favored by the incidence energy E (ρ_3 and ρ_4 in our example), such that the first exponential subregime is dominated by these two resonances. This becomes clearer when we choose the incidence energy E at intermediate points between ε_3 and ε_4, as we illustrate below.

Consider the special case of incidence just in the middle of the two resonances of the doublet, $E = (1/2)(\varepsilon_3 + \varepsilon_4)$. The $\ln\Delta$ vs t graph for this case at $x = 10.0$ nm is shown in Fig. 5(a), and the detail of the first exponential domain is displayed in Fig. 5(b). In this case, $|\rho_4/\rho_3|^2 = 1.05$, implying that the resonances $n = 3$ and $n = 4$ share the leading contribution in the first exponential subregime. We now see in the $\ln\Delta$ vs t graph an enhanced oscillatory structure with a well-defined period, which is indicated by T in Fig. 5(b) as the separation of two consecutive maxima of the probability density (note that the absolute value taken in the difference $1 - |\Psi/\phi|$ duplicates the frequency in the $\ln\Delta$ vs t graph, and hence the period T is taken in the form illustrated in the figure). A direct measurement on the graph gives the numerical value $T = 453.4$ fs, which corresponds to a frequency of $\Omega = 0.013857$ fs^{-1}. On the other hand, if we calculate a Rabi-type frequency from the difference between the incidence energy and the nearest resonance (in this case ε_3 and ε_4 since E is equidistant from both resonance levels) we obtain $w = |E - \varepsilon_3|/\hbar = |E - \varepsilon_4|/\hbar = 0.013854$ fs^{-1}. The two frequencies are essentially the same. This numerical agreement shows that the buildup oscillations have exactly the frequency associated with the difference between the incidence energy and the nearest resonance. The dramatic enhancement of the oscillations is due to a constructive interference of two oscillatory contributions with the same frequency.

As a final example, let us consider an arbitrary off-resonance incidence energy in the region between the two resonances ε_3 and ε_4, say, $E = \varepsilon_3 + 2\Gamma_3 = 326.28$ meV. The plot of $\ln\Delta$ vs t at the fixed position $x_f = 10.0$ nm for this incidence energy is shown in Fig. 6(a). The detailed structure of the first exponential domain is further emphasized in the amplification shown in Fig. 6(b) using a shorter time interval within the region of the first exponential subregime. In contrast to the previous cases, here the buildup exhibits a more complicated oscillatory pattern with irregular oscillations. However, as we show below, this apparently complicated behavior is a mix of periodic oscillations with well-defined frequencies that can be characterized by the differences between the incidence energy E and the interacting resonances ε_n lying in the vicinity of E. In order to clarify this, we include in this case calculations of the probability density in Fig. 7(a) where we measure the period of the main different contributions.

In Fig. 7(a) we plot $|\Psi/\phi|^2$ vs t at the fixed position $x_f = 10$ nm. The buildup exhibits wide oscillations of period T_3 around the stationary value, and secondary oscillations of smaller amplitude and period T_4 embedded on the main curve can also be appreciated. Direct measurements on the graphs of these periods give the values $T_3 = 1.376$ ps and $T_4 = 265.1$ fs,

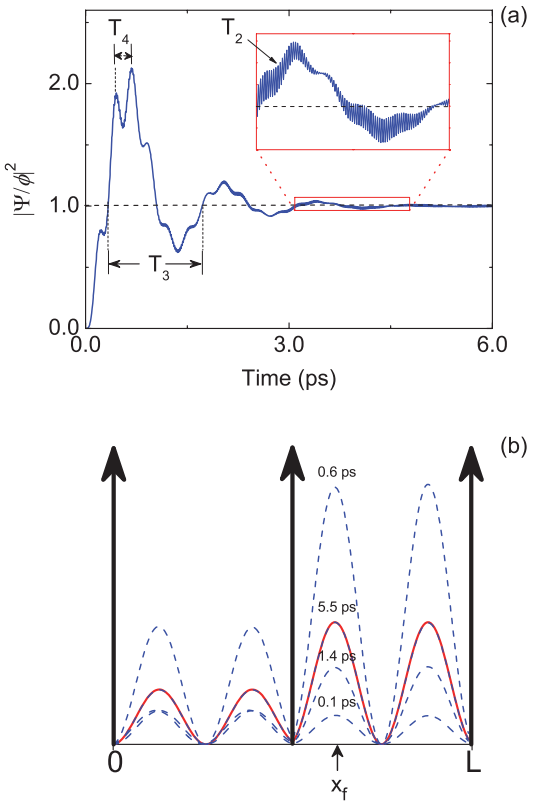

FIG. 7. (Color online) (a) Time evolution of $|\Psi/\phi|^2$ at the fixed position $x = 10$ nm for incidence at $E = \varepsilon_3 + 2\Gamma_3$ (blue solid line). The inset shows an expanded view of the curve. (b) Snapshots of $|\Psi|^2$ vs x at different fixed times (blue dashed lines) and incidence energy above the third resonance, $E = \varepsilon_3 + 2\Gamma_3$. The stationary probability density $|\phi|^2$ is included for comparison (red solid line).

which correspond respectively to the frequencies $\Omega_3 = 0.004\,567$ fs^{-1} and $\Omega_4 = 0.0237$ fs^{-1}. On the other hand, if we calculate the Rabi-type frequencies from the difference between the incidence energy E and the nearest resonances, we obtain $\omega_3 = |E - \varepsilon_3|/\hbar = 0.004\,564$ fs^{-1} and $\omega_4 = |E - \varepsilon_4|/\hbar = 0.0231$ fs^{-1}. As we can see, the Rabi-type frequencies ω_n are in excellent agreement with the measured ones Ω_n. An even finer oscillating structure is made evident in the expanded view of the curve shown in the inset of Fig. 7(a), in which we measure the period T_2 in the same fashion. We obtain the value $T_2 = 17.014$ fs, which gives $\Omega_2 = 0.369$ fs^{-1}, while the frequency obtained from the difference between E and the next-nearest-neighbor resonance becomes $\omega_2 = |E - \varepsilon_2|/\hbar = 0.366$ fs^{-1}, showing that the finer oscillations on the graph are produced by the interference of the incoming wave with faraway resonances belonging to the other doublet.

These frequencies are the absolute values of the quantities $\hat{\omega}_n$ that are explicitly given in Eqs. (14) and (15). Actually, if we plot $P(E,x,t)/|\phi|$ vs t using Eq. (11) with just $N = 4$ terms, we can reproduce almost exactly the graph of Fig. 7(a). Notice that other Rabi frequencies that come from the difference between resonance levels $\hat{\omega}_{mn}$ also appear in these equations; however, their role is very small. In quantum decay, on the other hand, only Rabi frequencies of the form $\omega_{mn} = |\hat{\omega}_{mn}| = |\varepsilon_m - \varepsilon_n|/\hbar$ are observed in the survival amplitude [29]. The Rabi-type oscillations with frequencies $\omega_n = |E - \varepsilon_n|/\hbar$ exhibited in our calculations occur only in the buildup process because they come from the interaction of the system's resonances and the incident wave of energy E, and physically correspond to oscillations of the probability density in the quantum wells of the system in a "breathing mode" at each point of the internal region during the buildup around the stationary value $|\phi|^2$, as illustrated in Fig. 7(b).

IV. CONCLUDING REMARKS

The exponential and nonexponential regimes of the buildup process in resonant tunneling structures were analyzed using explicit solutions of the time-dependent Schrödinger equation. For incidence at an isolated resonance, the buildup process exhibits a purely exponential behavior in a finite time interval, followed by a clear transition to a nonexponential time dependence. We show that the buildup of the probability amplitude in the nonexponential regime follows a time dependence that varies as $t^{-3/2}$, behaving exactly like the survival amplitude in quantum decay in the long-time regime [28]. In the exponential regime we distinguish two different situations depending on whether the incidence is chosen at the first resonance ($E = \varepsilon_1$) or at higher resonances ($E = \varepsilon_n$ with $n > 1$). In the former case, the exponential regime is dominated by the single resonance $E = \varepsilon_1$, and the probability amplitude grows at a rate dictated by the width Γ_1 of this resonance. For incidence at a higher isolated resonance, $E = \varepsilon_n$ ($n > 1$), it is found that the exponential regime is split into two subregimes: the first one is governed by the width Γ_n of the resonance chosen for the incidence energy, and the second one dominated by the width Γ_1 of the lowest resonance. The jump is directly from n to 1, and no intermediate stages associated with other resonant states m (with $1 < m < n$) are observed. The explanation of this behavior is given in our analysis in terms of the interaction of the incident wave with the system's resonances, represented by explicit coefficients in the analytic expression for the probability density derived in this work. Interestingly, this kind of dynamical behavior is quite similar to the time evolution of the survival amplitude in quantum decay when the initial state is placed at a higher resonance ($n > 1$) [29].

We also analyzed the buildup process in situations of incidence at resonance doublets. In this case, the exponential regime is also split into two subregimes, but the first one is dominated by two resonances instead of one, and the second subregime is governed by the width of the lowest resonance Γ_1. The competition of these two resonances for domination in the first exponential subregime is manifested as a mix of oscillations in the probability amplitude, with well-defined Rabi-type frequencies of the form $\omega_n = |E - \varepsilon_n|/\hbar$, where ε_n are the nearest resonances around the incidence energy E. Physically they correspond to oscillations around the stationary value $|\phi|^2$ of the probability density in the quantum wells of the system in a breathing mode at each point of the internal region during the transient regime of the buildup.

Our study was conducted in comparison with the well-known phenomenon of quantum decay, pointing out the similarities in the dynamical behavior of the relevant quantities of each case. Although there are striking similarities, there is an important difference worth stressing. Oscillations with frequencies of the form $\omega_{mn} = |\varepsilon_m - \varepsilon_n|/\hbar$ are present in both

the buildup and decay, but the Rabi-type oscillations with frequencies $\omega_n = |E - \varepsilon_n|/\hbar$ exhibited in our calculations occur only in the buildup process. The reason is simple: in quantum decay we have no incident wave of energy E.

The analysis presented here for the cases of $N = 2$ and $N = 3$ can be straightforwardly extended to describe the buildup dynamics in superlattices, where the process is expected to be much more complex due to the multiple interactions of the N resonances packed together in each miniband. This kind of analysis is relevant to a better understanding of the physics of how the electronic states are filled up with the incoming flux of particles in a quantum system according to its particular distribution of resonances.

ACKNOWLEDGMENTS

R.R. and J.V. acknowledge financial support from the Facultad de Ciencias UABC under Grant No. P/PIFI 2010-02MSU0020A-08, and A.H. acknowledges financial support from CITEC-UABC under Grant No. 332/1/N/122/16.

[1] A. del Campo, G. García-Calderón, and J. G. Muga, Phys. Rep. **476**, 1 (2009).
[2] D. K. Ferry and S. M. Goodnik, *Transport in Nanostructures* (Cambridge University Press, Cambridge, 1997).
[3] H. Mizuta and T. Tanoue, *The Physics and Applications of Resonant Tunneling Diodes* (Cambridge University Press, Cambridge, 1995).
[4] H. P. Simanjuntak and P. Pereyra, Phys. Rev. B **67**, 045301 (2003).
[5] S. L. Konsek and T. P. Pearsall, Phys. Rev. B **67**, 045306 (2003).
[6] Y. Fu and M. Willander, J. Appl. Phys. **97**, 094311 (2005).
[7] M. A. Andreata and V. V. Dodonov, J. Phys. A **37**, 2423 (2004).
[8] E. Granot and Marchewka, Europhys. Lett. **72**, 341 (2005).
[9] U. Wulf and V. V. Skalozub, Phys. Rev. B **72**, 165331 (2005).
[10] G. García-Calderón and A. Rubio, Phys. Rev. A **55**, 3361 (1997).
[11] M. Kleber, Phys. Rep. **236**, 331 (1994).
[12] R. Romo, Phys. Rev. B **66**, 245311 (2002).
[13] R. Romo and J. Villavicencio, Phys. Rev. B **60**, R2142 (1999).
[14] J. Villavicencio and R. Romo, Appl. Phys. Lett. **77**, 379 (2000).
[15] R. Romo and J. Villavicencio, Appl. Phys. Lett. **78**, 1769 (2001).
[16] J. A. Støvneng and E. H. Hauge, Phys. Rev. B **44**, 13582 (1991).
[17] Sergio Cordero, G. García-Calderón, R. Romo, and J. Villavicencio, Phys. Rev. A **84**, 042118 (2011).
[18] Y. G. Peisakhovich and A. A. Shtygashev, Phys. Rev. B **77**, 075326 (2008).
[19] Y. G. Peisakhovich and A. A. Shtygashev, Phys. Rev. B **77**, 075327 (2008).
[20] G. Gamow, Z. Phys. **51**, 204 (1928).
[21] R. W. Gurney and E. W. Condon, Phys. Rev. **33**, 127 (1929).
[22] L. A. Khalfin, Sov. Phys. JETP **6**, 1053 (1958).
[23] C. Rothe, S. I. Hintschich, and A. P. Monkman, Phys. Rev. Lett. **96**, 163601 (2006).
[24] S. R. Wilkinson, C. F. Bharucha, M. C. Fischer, K. W. Madison, P. R. Morrow, Q. Niu, B. Sundaram, and M. G. Raizen, Nature (London) **387**, 575 (1997).
[25] G. García-Calderón and J. Villavicencio, Phys. Rev. A **64**, 012107 (2001).
[26] G. García-Calderón, R. Romo, and A. Rubio, Phys. Rev. B **47**, 9572 (1993).
[27] *Handbook of Mathematical Functions*, edited by M. Abramowitz and I. A. Stegun (Dover, New York, 1965), p. 297; V. N. Fadeyeva and N. M. Tarent'ev, *Mathematical Tables* (Pergamon, London, 1961).
[28] G. García-Calderón and J. Villavicencio, Phys. Rev. A **73**, 062115 (2006).
[29] G. García-Calderón, J. L. Mateos, and M. Moshinsky, Ann. Phys. (NY) **249**, 430 (1996).